Published in final edited form as:
Glia. 2010 November 15; 58(15): 1858–1870. doi:10.1002/glia.21055.

ASTROCYTE-DERIVED GLUTATHIONE ATTENUATES HEMIN-INDUCED APOPTOSIS IN CEREBRAL MICROVASCULAR CELLS

Sangeetha Sukumari-Ramesh[1], **Melissa D. Laird**[1], **Nagendra Singh**[2], **John R. Vender**[1], **Cargill H. Alleyne Jr.**[1], and **Krishnan M. Dhandapani**[1,#]

[1] Department of Neurosurgery, Medical College of Georgia, Augusta, GA 30912

[2] Department of Biochemistry, Medical College of Georgia, Augusta, GA 30912

Abstract

Intracerebral hemorrhage (ICH) induces neurovascular injury via poorly defined mechanisms. The aim of the present study was to determine whether glio-vascular communication may restrict hemorrhagic vascular injury. Hemin, a hemoglobin by-product, concentration- and time-dependently increased apoptotic cell death in mouse bEnd.3 cells and in primary human brain microvascular endothelial cells, at least in part, via a caspase-3 dependent pathway. Cell death was preceded by a NFκB-mediated increase in inflammatory gene expression, including up-regulation of inducible nitric oxide synthase (iNOS) expression and activity. Functionally, inhibition of iNOS or the addition of a peroxynitrite decomposition catalyst reduced cell death. Interestingly, co-treatment with astrocyte conditioned media (ACM) reversed hemin-induced NFκB activation, nitrotyrosine formation, and apoptotic cell death, at least in part, via the release of the endogenous antioxidant, reduced glutathione (GSH). Prior treatment of astrocytes with the glutathione-depleting agent, DL-buthionine (S,R)-sulfoximine (BSO) or direct addition of diethyl maleate, a thiol depleting agent, to ACM reversed the observed protection. In contrast, neither exogenous GSH nor the GSH precursor, N-acetylcysteine, was protective in bEnd.3 cells. Together, these data support an important role for astrocyte-derived GSH in the maintenance of oxidative balance in the vasculature and suggest therapeutic targeting of the GSH system may reduce neurological injury following ICH.

Keywords

glia; anti-oxidant; neurovascular; GSH; blood-brain barrier

INTRODUCTION

Hemorrhagic stroke is a devastating neurological injury, accounting for 10–15% of all strokes and inducing ~50% mortality within the first month (Rincon and Mayer 2004). Intracerebral hemorrhage (ICH), the most common and least treatable form of hemorrhagic stroke, is induced by a ruptured blood vessel which results in the accumulation of blood within the parenchyma. The resultant hematoma contributes to neurovascular dysfunction by reducing cerebral blood flow (CBF), disrupting the blood-brain barrier (BBB), increasing vasogenic edema and promoting delayed neurological injury (Christoforidis et al. 2007; Davis et al. 2006); however, the cellular mechanisms underlying these actions remain incompletely understood and contribute to the dearth of treatment options following ICH.

[#]Address correspondence to: Krishnan M. Dhandapani, Ph.D., Department of Neurosurgery, Medical College of Georgia, Tel: (706) 721-8846, Fax: (706) 721-7619, kdhandapani@mcg.edu.

Acute endothelial injury and vascular inflammation are predictive markers of subsequent hematoma enlargement and the development of vasogenic edema (Silva et al. 2005; Wasserman et al. 2007), thus, a reduction in neurovascular injury may improve clinical outcomes after ICH. In support of this contention, apoptosis of cerebral endothelial cells increased BBB permeability, vasogenic edema, and neurological impairment following hemorrhagic stroke (Doczi 1985; Park et al. 2004). Similarly, perivascular activation of the pro-inflammatory transcription factor, NFκB, correlated with the expression of inducible nitric oxide synthase (iNOS) and increased apoptosis within perihematoma blood vessels after ICH (Hickenbottom et al. 1999; Nakamura et al. 2000). The production of nitric oxide (NO) by iNOS promotes neuroinflammation, oxidative stress, and BBB disruption following brain injury (Forster et al. 1999), further suggesting a reduction in vascular injury may improve patient prognoses after ICH.

The Neurovascular Unit (NVU) consists of neurons, glia, and microvascular cells organized into discreet functional units. Astrocytes, the predominant cell type within the NVU, are anatomically in juxtaposition to endothelial cells. Astrocytic end feet contact over 90% of the cerebrovascular surface, allowing glio-vascular communication essential for the maintenance of the BBB, regulation of CBF, and control of oxidative balance (Janzer and Raff 1987; Takano et al. 2006; Wilson 1997). Interestingly, administration of a gliotoxin to induce focal astrocyte loss acutely increased microvascular damage and disrupted the BBB in rats (Willis et al. 2004), suggesting astrocytes maintain microvascular function and survival under basal conditions; however, the functional role(s) of astrocytes following ICH remains largely unexplored.

In the present study, we examined whether astrocyte-derived soluble factors reduce microvascular injury following exposure to hemin, a hemoglobin oxidation product that accumulates within intracranial hematomas (Letarte et al. 1993). Our data implicate astrocyte-derived reduced glutathione (GSH) in the reduction of hemin-induced endothelial cell apoptosis. These findings may have direct mechanistic relevance for understanding secondary brain injury, including disruption of the BBB and development of vasogenic edema, following ICH.

MATERIALS AND METHODS

Materials

Hemin was purchased from USB Corporation (Cleveland, OH). Peroxynitrite was purchased from Cayman Chemicals (Ann Arbor, MI) and helenalin was obtained from Biomol (Plymouth Meeting, PA). The peroxynitrite decomposition catalyst, FeTPPS (5,10,15,20-tetrakis-[4-sulfonatophenyl]-porphyrinato-iron[III]), aminoguanidine, and pyrrolidine dithiocarbamate (PDTC) were purchased from Calbiochem (La Jolla, CA). Trolox was obtained Tokyo Chemical Industry, Co. (Portland, OR). Iminopiperdine was purchased from Tocris Bioscience (Ellisville, MO). All cell culture supplies were from Hyclone (Logan, UT)

Cell Culture

Mouse bEnd.3 cerebral microvascular cells (Montesano et al. 1990) were purchased from ATCC (Manasaas, VA) and cultured in Dulbecco's modified Eagle medium (DMEM) supplemented with fetal bovine serum and antibiotics. Primary astrocyte cultures were obtained from the cerebral cortices of 1–2 day old CD-1 mice, per our laboratory (Laird et al. 2008). Upon reaching confluence, cells were treated with 8 μM cytosine arabinoside for one week followed by a 1.5h exposure to 50 mM leucine methyl ester to eliminate microglia. Cultures were routinely >98% astrocytes, as assessed by immunocytochemistry using the astrocyte-specific marker, glial fibrillary acidic protein (GFAP) and <1%

microglia, as assessed by the microglial marker, CD11b. Astrocytes were used for experiments between days 28–35 *in vitro*. Astrocyte-conditioned media (ACM) was collected in serum-free DMEM after a 24h exposure and stored at −80°C.. All experimental treatments were performed in serum-free media, which did not adversely affect cellular viability. Human brain microvascular endothelial cells and human astrocytes (Sciencell Research Laboratories, Carlsbad, CA) were cultured per supplier's recommendations.

Cell death assays

The MTT (3-[4,5-dimethylthiazol-2-yl]-2,5-diphenyltetrazolium bromide) reduction assay and lactate dehydrogenase (LDH) release assays were performed as detailed by our laboratory (Dhandapani and Brann 2003; Dhandapani et al. 2007). Cell death was also quantified by flow cytometry. Briefly, following treatments, floating and adherent cells were collected and washed. Cell suspensions were then stained for 15 minutes at room temperature with annexin V-PE (BD Pharmigen, San Diego, CA), an early apoptotic marker, and with 7-AAD, a cell death marker which is excluded by viable cells, but penetrates the cell membrane of dead or dying cells. The percentage of apoptotic cells was quantified using a FACScan flow cytometry.

Western blotting

Whole cell lysates were collected in radioimmunoprecipitation (RIPA) buffer containing protease inhibitor cocktail, phosphatase-inhibitor cocktail, and phenyl methane sulfonyl fluoride (PMSF) and quantified by BCA protein assay (Pierce, Rockford, IL). 30 μg of protein were resolved on a 4–20% sodium dodecyl sulfate-polyacrylamide gel and transferred onto a polyvinylidene difluoride (PVDF) membrane. Blots were incubated overnight at 4°C in anti-cleaved-caspase-3 primary antibody (1:1000; Cell Signaling Technology, Beverly, MA) or anti-PARP primary antibody (1:1000; Cell Signaling Technology, Beverly, MA), which detects both cleaved and full length PARP, followed by 2h incubation with an Alexa Fluor 750 secondary antibody at room temperature. Blots were visualized using a Li-Cor Odyssey near-infrared imaging system and densitometry analysis was performed using Quantity One software (Bio-Rad, Foster City, CA).

GSH quantification

Reduced glutathione (GSH) was measured, as described by our laboratory (Laird et al. 2008). Briefly, cultures were washed in PBS, then incubated for 0.5h at 37°C with 100 μM monochlorobimane (Invitrogen, Carlsbad, CA), followed by lysis in 0.2% Triton X-100 in PBS. Protein concentrations in the supernatant were measured by BCA assay. Changes in the fluorescence as a result of the formation of GSH-monochlorobimane adduct in the supernatant was measured at $\lambda_{excitation}$ =380 nm and $\lambda_{emission}$ =478 nm. GSH concentrations were quantified using a standard curve and normalized to protein content to control for differences in cell number between wells.

Nitrite assay

Nitrite levels in culture supernatants, an indirect measure of NO formation, were quantified using a Greiss Reagent Assay (Promega, Madison, WI). Samples were assayed in triplicate and data was expressed as the concentration of nitrite accumulated over a time course (normalized to total protein).

Measurement of lipid peroxidation

Lipid peroxidation was assessed by measuring the formation of malondialdehyde (MDA), per our laboratory (Laird et al. 2008). Briefly, cell homogenate (100 μL) was added to a reaction mixture containing 100 μL of 8.1% sodium dodecyl sulfate (SDS), 750 μL of 20%

acetic acid (pH 3.5), 750 μL of 0.8% thiobarbituric acid and 300 μL of distilled water. Samples were boiled for 1h, and then centrifuged at 4000*xg* for 10 minutes. The absorbance of the supernatant was measured by spectrophotometry at 650 nm and normalized to total protein content. TBARS formation, a measure of oxidative stress and lipid peroxidation, was expressed as nmol/mg protein.

NFκB binding assays

Nuclear extracts were prepared using a Nuclear Extract Kit (Active Motif, Carlsbad, CA). 7.5 μg of nuclear extract were used to determine NFκB activation (TransAM, Active Motif, Carlsbad, CA) (Dhandapani et al. 2007; Laird et al. 2008). This method rapidly detects activated NFκB complex binding (p50 or p65 subunits), possessing a detection limit of <0.5 μg nuclear extract or <0.4 ng recombinant p50 or p65 protein/well. Nuclear extracts prepared from TPA-stimulated Jurkat cells (2.5 μg/well) were used as a positive control. To demonstrate binding specificity, a 20-fold excess of an NFκB wild type consensus oligonucleotide (20 pmol/well) was used as a competitor to block specific NFκB binding to the well. Conversely, a mutated consensus NFκB oligonucleotide had no effect on NFκB binding, demonstrating the specificity of the reaction.

RNA isolation and qRT-PCR

Total RNA was isolated using a SV RNA Isolation Kit (Promega, Madison, WI). qRT-PCR was performed on a SmartCycler (Cepheid, Sunnyvale, CA) using a SuperScript III Platinum SYBR Green One-Step qRT-PCR kit (Invitrogen, Carlsbad, CA). Primers sequences were as follows: iNOS: (FP 5′-CCTTGTTCAGCTACGCCTTC-3′; RP 5′-AAGGCCAAACACAGCATACC-3′), ICAM: (FP 5′-TTCACACTGAATGCCAGCTC-3′; RP 5′-GTCTGCTGAGACCCCTCTTG-3′), VCAM-1: (FP 5′-ATTTTCTGGGGCAGGAAGTT-3′; RP 5′-ACGTCAGAACAACCGAATCC-3′), IL-1β: (FP 5′-GCCCATCCTCTGTGACTCAT-3′; RP 5′-AGGCCACAGGTATTTTGTCG-3′), COX-2: (FP 5′-AGAAGGAAATGGCTGCAGAA-3′; RP 5′-GCTCGGCTTCCAGTATTGAG-3′), TNF-α: (CGTCAGCCGATTTGCTATCT-3″; RP 5′-CGGACTCCGCAAAGTCTAAG-3′), IL-6: (FP 5′-AGTTGCCTTCTTGGGACTGA-3′; RP 5′-TCCACGATTTCCCAGAGAAC-3′), RPS3 (FP 5′-AATGAACCGAAGCACACCATA-3′; RP 5′-ATCAGAGAGTTGACCGCAGTT-3′). Data were quantified using serial cDNA dilutions and normalized to the housekeeping gene, RPS3, which was unaffected by experimental treatment. Data were expressed as fold change versus vehicle-treated cultures. Primer specificity was confirmed by melting curve analysis and electrophoresis of PCR products on a 2% agarose gel to confirm the presence of a single band of the predicted size.

Statistical analysis

Data were analyzed using by one-way analysis of variance (ANOVA) followed by Student Newman Keul's or Dunnett's post-hoc test, as indicated in the Figure Legends. Experiments were performed in triplicate to verify results. Data are expressed as mean ± SEM. A p value <0.05 was considered statistically significant.

RESULTS

Hemin induces cell death in microvessel cells

Hemin concentration-dependently (5–75 μM) decreased the viability of mouse bEnd.3 cerebral microvascular cells (Figure 1A) or human brain microvascular cells (Figure 1B). A significant reduction in viability was noted 6h after treatment with 30 μM hemin ($p<0.05$ vs. vehicle) and a maximal effect observed after an 18h treatment with 75 μM hemin (58 ±

4.7% reduction in viability; $p<0.01$ vs. vehicle). An 18h treatment with 30 μM hemin reduced cellular viability by ~50% ($p<0.01$ vs. vehicle), justifying the subsequent use of this time point and concentration. Vehicle (0.1 N NaOH) did not significantly reduce cellular viability at any time point.

Co-treatment of hemin with the antioxidant, ascorbic acid (100, 250, 500 μM), concentration-dependently maintained cellular viability at 69.4 ± 3.1%, 77.6 ± 2.6% or 96.9 ± 3.9% of vehicle, respectively ($p<0.05$, 100 μM vs. hemin; $p<0.01$, 250 or 500 μM vs. hemin) (Figure 1C). Similarly, trolox (250, 500, 1000 μM) significantly increased cellular viability to 68.9 ± 2.3%, 81.1 ± 2.4% or 96.6 ± 2.9% of vehicle, respectively ($p<0.05$, 250 μM vs. hemin; $p<0.01$, 500 or 1000 μM vs. hemin) (Figure 1D). Desferrioxamine (DFO), an iron chelator, also maintained cellular viability at 66.7 ± 3.7%, 82.4 ± 3.1%, or 89.1 ± 3.7% of vehicle, at concentrations of 100, 200 or 400 μM DFO, respectively ($p<0.05$, 100 μM vs. hemin; $p<0.01$, 200 or 400 μM vs. hemin) (Figure 1E), supporting a role for iron-mediated oxidative stress in hemin-induced vascular injury.

Astrocytic soluble factors limit hemin-induced microvessel apoptosis

Hemin-induced microvessel cell death was reduced from 54.9 ± 3.0% viability (hemin alone) to 98.3 ± 3.5% viability when hemin exposure was performed in the presence of ACM ($p<0.001$ vs. hemin, not significantly different from vehicle) (Figure 2A). Cellular proliferation, as assessed by the BrDU incorporation assay, was not significantly changed following ACM treatment of bEnd.3 cells, suggesting the increase in MTT reduction reflected increased cellular viability (data not shown). This assertion was further supported by data showing ACM significantly attenuated hemin-induced LDH release (Figure 2B). Similarly, hemin increased Annexin-V labeling and this effect was completely prevented in the presence of ACM (Figure 2C). Co-treatment with ACM also prevented the damaging effects of hemin, preserving a healthy cellular morphology comparable to vehicle-treated cultures (Figure 2D). Notably, neither protein denaturation nor size exclusion filtration of soluble factors larger than 10 kDa reduced the protective capacity of ACM after hemin treatment, suggesting a small, proteinaceous factor within ACM may mediate the observed vasculoprotection (Figure 2A,B).

Hemin (30 μM, 18h treatment) dramatically increased cleaved caspase-3 (Figure 3A) and increased the cleavage of PARP, a downstream target of caspase-3 (Figure 3B). These effects were blocked when hemin was incubated in the presence of ACM, suggesting astrocyte-derived soluble factors limit apoptotic activation. Accordingly, the cell permeable, irreversible caspase-3 inhibitor, Z-VAD.fmk (100 μM) significantly reduced hemin-induced cell death (81.9 ± 6.8% viability in hemin + Z-VAD.fmk vs. 52.8 ± 5.8% in hemin only; $p<0.01$ vs. hemin treatment, $p<0.05$ vs. vehicle) (Figure 3C). Consistent with this effect, Z-VAD.fmk (100 μM) attenuated caspase-3 activation and blocked PARP cleavage (Figure 3D).

GSH mediates the protective capacity of ACM

Soluble factors within ACM reversed oxidative hemin toxicity in microvascular cells; however, the identity of the protective factor(s) remained undetermined. Collection of ACM following an 8h treatment with the GSH-depleting agent, DL-buthionine (S,R)-sulfoximine (BSO; 1 mM) reversed the protective effects of ACM on cellular viability (Figure 4A) and caspase-3 activation (Figure 4B) after hemin treatment (not significantly different from hemin, $p<0.01$ vs. ACM). Conversely, direct addition of BSO (1 mM) to previously collected ACM had no effect on bEnd.3 cellular viability as compared to ACM alone, demonstrating the effect of BSO was mediated by astrocytes and not directly at the level of the microvessel. These data also support the possibility that astrocyte-derived GSH limits

caspase-3 activation following hemin treatment. Consistent with this hypothesis, ACM collected following an 8h treatment with BSO exhibited a 74.3 ± 3.5% reduction in GSH content as compared with ACM ($p<0.001$ vs. ACM) (Figure 4C); however, BSO treatment had no effect on the viability of astrocyte cultures, suggesting the effect of BSO was at the level of GSH depletion rather than a reflection of toxicity. In contrast, the direct addition of BSO to previously collected ACM did not significantly reduce GSH content within ACM (Figure 4C). Finally, addition of the thiol-depleting agent, diethyl maleate (DM; 300 μM) completely reversed the protective effect of ACM following hemin treatment (97.8 ± 4.8% in ACM vs. 58.4 ± 6.2% of control viability in ACM +DM; $p<0.01$) (Figure 4D), whereas DM alone did not significantly affect hemin toxicity in microvessel cells.

Treatment of bEnd.3 cells with exogenous GSH attenuated hemin-induced cell death after an 18h treatment (Figure 5). 100 μM GSH significantly increased cellular viability to 69.5 ±7.0% of control ($p<0.05$ vs. hemin treatment). Higher concentrations of GSH further increased cellular viability, with full protection observed by co-treatment with 1 mM GSH (96.0 ± 6.1% viability; $p<0.01$ vs. hemin treatment). The GSH precursor drug, N-acetyl-L-cysteine (NAC; 500 μM) also reduced hemin toxicity, increasing cellular viability to 80.1 ± 4.3% of control ($p<0.05$ vs. hemin treatment), with full protection noted with 1 mM NAC treatment (95.7 ± 3.9%; $p<0.01$ vs. hemin treatment). Co-treatment with cysteine, a key GSH precursor required by endothelial cells for endogenous GSH synthesis was also protective; albeit to a lesser extent that GSH. A significant and maximal protection was observed following treatment with 750 μM cysteine (74.1 ± 8.0% viability; $p<0.05$ vs. hemin treatment). In contrast, neither GSSG nor cystine, which lack free thiol groups, were protective at any concentration tested.

Peroxynitrite mediates microvessel injury following hemin treatment

GSH limits peroxidative vascular injury; thus, the possible contribution of peroxynitrite formation toward hemin toxicity was investigated. Co-treatment with FeTPPS (25 μM), a peroxynitrite decomposition catalyst, significantly attenuated hemin-induced cell death (87.1 ± 1.8% of control viability; $p<0.01$ vs. hemin). Higher concentrations (50, 100 μM) of FeTPPS similarly increased cellular viability to 95.6 ± 3.3 % and 99.4 ± 4.1% of control, respectively ($p<0.01$ vs. hemin) (Figure 6A). Authentic peroxynitrite (500 μM) decreased viability within 6h, with a significant effect observed after an 18h treatment. Both 750 and 1000 μM peroxynitrite reduced cellular viability within 3h, with a larger reduction in viability noted at 6h and 18h ($p<0.01$ vs. hemin) (Figure 6B). Hemin increased the formation of nitrotyrosine, a marker of peroxidative injury, by 3.9 ± 0.7 fold over vehicle-treated cultures ($p<0.01$). In contrast, hemin-induced nitrotyrosine formation was reversed by co-treatment with ACM (1.2 ± 0.6 fold increase; $p<0.01$ vs. hemin) (Figure 6C). Similarly, the hemin-induced increase in TBARS formation, a marker of lipid peroxidation (0.33 ± 0.05 nmol TBARS/mg protein in vehicle-treated cultures vs. 0.89 ± 0.13 nmol TBARS/mg protein following hemin treatment; $p<0.05$ vs. vehicle) was completely reversed by ACM (0.26 ± 0.10 nmol TBARS/mg protein; $p<0.05$ vs. hemin treatment) (Figure 6D).

iNOS contributes to hemin-induced microvessel toxicity

Hemin (30 μM) significantly increased the expression of inflammatory genes, including COX-2, IL-1β, iNOS, TNF-α, VCAM-1, and ICAM-1 (Figure 7A). Of particular interest, hemin induced a 2.6 ± 0.3 fold upregulation in iNOS mRNA expression ($p<0.05$ vs. vehicle). The effect of hemin on inflammatory gene expression and NFκB binding was unaffected by co-incubation with polymixin B (10 μg/mL), suggesting residual endotoxin within the hemin preparation did not account for the observed pro-inflammatory effects (data not shown). The NFκB inhibitors, PDTC (100 μM) or helenalin (10 μM), significantly attenuated hemin-induced inflammatory gene expression, indicating a possible mediatory

role for NFκB. As was observed with gene expression, hemin increased nitrite production, a measure of iNOS activity, within 3h of treatment ($p<0.05$ vs. vehicle), with a maximal effect at 6h, the latest time point investigated ($p<0.01$ vs. vehicle) (Figure 7B). Consistent with a reduction in iNOS expression and activity, NFκB inhibition with either PDTC or helenalin completely reversed hemin-induced nitrite formation (Figure 7B). Functionally, co-treatment with the iNOS inhibitors, aminoguanidine (Figure 7C) or iminopiperdine (Figure 7D) attenuated hemin toxicity. Aminoguanidine (0.5 mM) significantly reduced hemin toxicity by 14.1% ($p<0.05$ vs. hemin), with a 37.7% reduction in cell death observed after treatment with 2 mM aminoguanidine ($p<0.01$ vs. hemin). Iminopiperdine (200 μM) also effectively reduced hemin-induced cell death ($p<0.001$ vs. hemin).

NFκB is required for hemin toxicity

Hemin (30 μM) stimulated the DNA binding activity of both the p50 and p65 subunits of NFκB in bEnd.3 cells (2.7 ± 0.6 fold increase and 2.2 ± 0.6 fold increase vs. vehicle, respectively; $p<0.05$) (Figure 8A). ACM completely reduced the stimulation of both subunits after hemin treatment (1.2 ± 0.3 fold increase and 1.3 ± 0.3 fold vs. vehicle, respectively; not significantly different from vehicle, $p<0.05$ vs. hemin treatment). ACM collected from BSO-treated astrocytes did not attenuate hemin-induced NFκB activation, further supporting a functional role for astrocyte-derived GSH in limiting hemin-induced vascular injury (Figure 8B). Consistent with these findings in bEnd.3 cells, conditioned media collected from primary human astrocyte cultures similarly reduced activation of p50 and p65 in primary human brain microvascular endothelial cells (Figure 8C). As was observed in murine cells, treatment of human astrocytes with BSO prior to ACM collection prevented the ability of astrocytes to limit vascular NFκB activation (Figure 8D). Functionally, inhibition of NFκB using curcumin or PDTC, treatment with the p65 translocation inhibitor, helenalin, or incubation with the IKK inhibitor, wedelolactone, significantly reduced hemin-induced cell death in bEnd.3 cells (Figure 9A–C).

DISCUSSION

Neurovascular interactions are complex and poorly understood, contributing to a lack of viable therapeutic options after ICH. A key determinant of patient prognosis is acute hematoma expansion, which increases multifocal bleeding and clinical deterioration. Although hemolytic clot breakdown may attenuate the mass lesion, this process also increases the sustained accumulation of cytotoxic hemoglobin byproducts within the parenchyma, activates a prolonged inflammatory response, and induces neurological deterioration (Bhasin et al. 2002; Hua et al. 2000; Letarte et al. 1993). The present study reports a novel mechanism whereby astrocyte-derived GSH attenuates vascular inflammation and peroxidative cell death in mouse and human brain microvascular endothelial cells after a hemorrhagic injury. These data support therapeutic targeting of astrocytes to maintain oxidative balance and reduce neurological injury after ICH.

Apoptosis is regarded as the primary form of cell death in the perihematomal region in pre-clinical models and in post-mortem human studies (Matsushita et al. 2000; Qureshi et al. 2001). Hemin, a toxic hemoglobin oxidation product, induced apoptotic cell death in mouse and human microvascular cells using concentrations that were <10% of those observed in an intracranial hematoma (Letarte et al. 1993). This effect was correlated with caspase-3 activation and cleavage of the caspase-3 substrate, PARP; however, it is notably that the irreversible, pan-caspase inhibitor, Z-VAD.fmk, partially attenuated hemin-induced cell death. Consistent with this result, Z-VAD.fmk reduced hemin-induced caspase-3 activation in bEnd.3 cells by 46%, although PARP cleavage was fully reversed to vehicle levels. Although unexpected, this finding is consistent with a report showing Z-VAD.fmk only partially inhibited caspase-3 activation after 7-ketocholesterol treatment in R28 retinal

neurosensory cells (Neekhra et al. 2007). Thus, we cannot exclude the possibility that hemolytic degradation may induce vascular damage via both caspase-dependent and -independent pathways.

Focal astrocyte loss increased basal microvascular damage and BBB dysfunction (Willis et al. 2004). Astrocytic cell death was also observed within the white matter of pre-term infants after an intraventricular hemorrhage (Chamnanvanakij et al. 2002) and loss of astrocytes within the perihematoma region temporally preceded vascular injury after experimental ICH (Gong et al. 2001; Wasserman et al. 2007). These findings raise the unexplored possibility that glial cell loss may remove a key source of protective factors resulting in increased neurovascular damage and a poor clinical outcome after ICH. Consistent with this assertion, microvessel cell death was completely reversed when hemin treatment was performed in the presence of ACM, suggesting a soluble, astrocyte-derived factor(s) attenuates hemin-induced peroxidative injury. Characterization of ACM revealed that GSH, an abundant tripeptide and the principal non-enzymatic antioxidant within the brain, mediated, at least in part, the protective capacity of astrocytes. Astrocytes, the primary source of GSH within the brain, maintain intracellular concentrations between 1–5 mM *in vivo* and release up to 10% of this pool hourly (Sagara et al. 1996). Addition of exogenous GSH at concentrations within the range released by astrocytes *in vivo*, significantly reduced subsequent hemin toxicity whereas equimolar concentrations of GSSG, which lack a free thiol group, failed to reverse cell death.

Based on the reported ability of GSH to attenuate peroxidative endothelial damage (Bai et al. 2001; Nakamura et al. 2000), astrocytic GSH may attenuate neurovascular injury after ICH. This possibility is supported by the finding that pharamacological depletion of cerebral GSH promotes microvascular dysfunction (Agarwal and Shukla 1999) and peripheral administration of the thiol depleting agent, diethyl maleate, reduced cortical GSH content and increased the generation of superoxide, a precursor for peroxynitrite synthesis (Gupta et al. 2000). In agreement with these findings, hemin, at concentrations used in this study, rapidly depleted intracellular GSH and induced necroptotic cell death in cultured astrocytes (Laird et al. 2008). As removal of GSH significantly attenuated the protective capacity of ACM against hemin-induced microvascular cell death, these data implicate an important role for astrocyte-derived GSH in limiting vascular injury and suggest acute astrocytic loss may remove the predominant source of GSH, resulting in increased neurovascular injury after exposure to hemoglobin-derived oxidation products.

The mechanisms underlying the protective capacity of astrocyte-derived GSH after hemin treatment remain unclear. Exogenous GSH and to a lesser extent, cysteine, reduced hemin toxicity whereas neither GSSG nor cystine (which lack free thiol groups) significantly influenced cellular viability. Cysteine may be oxidized in the extracellular space to form cystine, which can then be transported into cells and reduced prior to GSH synthesis (Wu et al. 2004). Thus, the inability of exogenous cystine, to limit cell death suggests new GSH synthesis within vascular cells is an unlikely mechanism of protection. Coupled with the ability of the thiol-depleting agent, diethyl maleate, to completely reverse the protective ability of ACM, these studies implicate an extracellular mechanism of protection by GSH. Although unexplored in this report, it is notable that GSH enhances hemin degradation *in vitro* (Zou et al. 2002). Additionally, GSH may function as an ‘NO sink’, preferentially combining with NO to form nitrosglutathione (GSNO) rather than permitting the formation of the highly damaging oxidant, peroxynitrite. These possible protective actions of GSH remain completely unexplored after ICH; however, it is noteworthy that GSNO attenuates vasoconstriction and brain injury after subarachnoid hemorrhage (SAH) (Sehba et al. 1999; Sehba et al. 2007).

The Nrf2 transcription factor reduced oxidative stress, immune infiltration, and neurological injury following ICH (Nakamura et al. 2000) whereas Nrf2-deficient mice exhibited an increase in oxidative stress and worse neurological outcome as compared to wild-type mice (Nakamura et al. 2000; Wang and Dore 2007). The protective mechanism of Nrf2 was not established in these reports; however, Nrf2 regulates glutamate-cysteine ligase (GCL) and glutathione synthetase, two enzymes which are required for GSH biosynthesis. Nrf2-induced gene expression is preferentially activated in astrocytes (Kraft et al. 2004; Lee et al. 2003) and the neuroprotective effects of Nrf2 were dependent upon increased GSH biosynthesis within astrocytes (Kraft et al. 2004; Shih et al. 2003). Although experimental validation of GSH as a mediator of Nrf2-induced protection after ICH remains to be demonstrated, these data are consistent with our previous work showing hemin induced acute astrocytic death following GSH depletion (Laird et al. 2008) and further suggest that therapeutic targeting of Nrf2 may limit neurovascular damage after a brain hemorrhage.

Activation of the pro-inflammatory transcription factor, NFκB, was observed in dying cells and correlated with iNOS expression after ICH (Hickenbottom et al. 1999; Nakamura et al. 2000). Consistent with this notion, hemin-induced microvessel toxicity was dependent upon NFκB activation and subsequent iNOS expression. Peroxynitrite, which often mediates the damaging effects of iNOS, is formed via the equimolar reaction of NO and superoxide (Beckman et al. 1990; Phares et al. 2007). Upregulation of the superoxide generating enzyme, NADPH oxidase, within the microvasculature was associated with disruption of the BBB, development of vasogenic edema, and a poor outcome after ICH (Lu et al. 2006). In contrast, genetic overexpression of superoxide dismutase reduced cortical iNOS expression and attenuated peroxidative damage after SAH (McGirt et al. 2002; Saito et al. 2001). Thus, these reports are in agreement with our finding that hemin toxicity was prevented by a peroxynitrite degradation catalyst or with apocynin, a superoxide inhibitor (data not shown). Furthermore, the rapid depletion of intracellular GSH and induction of microvessel cell death are consistent with reports linking peroxynitrite formation with neurovascular dysfunction, BBB opening, and the development of vasogenic edema (Oury et al. 1993; Phares et al. 2007; Szabo et al. 2002).

The present studies document a novel protective role for astrocyte-derived GSH in limiting hemorrhagic injury in human and mouse cerebral microvessel cells and raise the interesting possibility that acute astrocytic injury contributes to subsequent neurovascular damage following ICH. Future studies by our group will assess the protective role of astrocyte-derived GSH in a pre-clinical animal model, which may better recapitulate the events after ICH in humans. Given the temporal delay between a brain hemorrhage and secondary brain injury, therapeutic targeting of the glial GSH system may represent a novel therapeutic strategy, which could potentially be implemented within a clinically-reasonable therapeutic window.

Acknowledgments

The authors work was supported in part by grants from the National Institute of Health (NS065172) and American Heart Association (BGIA2300135) to KMD and by a fellowship from the American Heart Association (PRE2250690) to MDL

References

Agarwal R, Shukla GS. Potential role of cerebral glutathione in the maintenance of blood-brain barrier integrity in rat. Neurochem Res. 1999; 24(12):1507–14. [PubMed: 10591399]

Bai Y, Suzuki AK, Sagai M. The cytotoxic effects of diesel exhaust particles on human pulmonary artery endothelial cells in vitro: role of active oxygen species. Free Radic Biol Med. 2001; 30(5): 555–62. [PubMed: 11182526]

Beckman JS, Beckman TW, Chen J, Marshall PA, Freeman BA. Apparent hydroxyl radical production by peroxynitrite: implications for endothelial injury from nitric oxide and superoxide. Proc Natl Acad Sci U S A. 1990; 87(4):1620–4. [PubMed: 2154753]

Bhasin RR, Xi G, Hua Y, Keep RF, Hoff JT. Experimental intracerebral hemorrhage: effect of lysed erythrocytes on brain edema and blood-brain barrier permeability. Acta Neurochir Suppl. 2002; 81:249–51. [PubMed: 12168318]

Chamnanvanakij S, Margraf LR, Burns D, Perlman JM. Apoptosis and white matter injury in preterm infants. Pediatr Dev Pathol. 2002; 5(2):184–9. [PubMed: 11910514]

Christoforidis GA, Slivka A, Mohammad Y, Karakasis C, Avutu B, Yang M. Size matters: hemorrhage volume as an objective measure to define significant intracranial hemorrhage associated with thrombolysis. Stroke. 2007; 38(6):1799–804. [PubMed: 17463318]

Davis SM, Broderick J, Hennerici M, Brun NC, Diringer MN, Mayer SA, Begtrup K, Steiner T. Hematoma growth is a determinant of mortality and poor outcome after intracerebral hemorrhage. Neurology. 2006; 66(8):1175–81. [PubMed: 16636233]

Dhandapani K, Brann D. Neuroprotective effects of estrogen and tamoxifen in vitro: a facilitative role for glia? Endocrine. 2003; 21(1):59–66. [PubMed: 12777704]

Dhandapani KM, Mahesh VB, Brann DW. Curcumin suppresses growth and chemoresistance of human glioblastoma cells via AP-1 and NFkappaB transcription factors. J Neurochem. 2007; 102(2):522–38. [PubMed: 17596214]

Doczi T. The pathogenetic and prognostic significance of blood-brain barrier damage at the acute stage of aneurysmal subarachnoid haemorrhage. Clinical and experimental studies. Acta Neurochir (Wien). 1985; 77(3–4):110–32. [PubMed: 4072781]

Forster C, Clark HB, Ross ME, Iadecola C. Inducible nitric oxide synthase expression in human cerebral infarcts. Acta Neuropathol. 1999; 97(3):215–20. [PubMed: 10090667]

Gong C, Boulis N, Qian J, Turner DE, Hoff JT, Keep RF. Intracerebral hemorrhage-induced neuronal death. Neurosurgery. 2001; 48(4):875–82. discussion 882–3. [PubMed: 11322448]

Gupta A, Gupta A, Datta M, Shukla GS. Cerebral antioxidant status and free radical generation following glutathione depletion and subsequent recovery. Mol Cell Biochem. 2000; 209(1–2):55–61. [PubMed: 10942201]

Hickenbottom SL, Grotta JC, Strong R, Denner LA, Aronowski J. Nuclear factor-kappaB and cell death after experimental intracerebral hemorrhage in rats. Stroke. 1999; 30(11):2472–7. discussion 2477–8. [PubMed: 10548686]

Hua Y, Xi G, Keep RF, Hoff JT. Complement activation in the brain after experimental intracerebral hemorrhage. J Neurosurg. 2000; 92(6):1016–22. [PubMed: 10839264]

Janzer RC, Raff MC. Astrocytes induce blood-brain barrier properties in endothelial cells. Nature. 1987; 325(6101):253–7. [PubMed: 3543687]

Kraft AD, Johnson DA, Johnson JA. Nuclear factor E2-related factor 2-dependent antioxidant response element activation by tert-butylhydroquinone and sulforaphane occurring preferentially in astrocytes conditions neurons against oxidative insult. J Neurosci. 2004; 24(5):1101–12. [PubMed: 14762128]

Laird MD, Wakade C, Alleyne CH Jr, Dhandapani KM. Hemin-induced necroptosis involves glutathione depletion in mouse astrocytes. Free Radic Biol Med. 2008; 45(8):1103–14. [PubMed: 18706498]

Lee JM, Calkins MJ, Chan K, Kan YW, Johnson JA. Identification of the NF-E2-related factor-2-dependent genes conferring protection against oxidative stress in primary cortical astrocytes using oligonucleotide microarray analysis. J Biol Chem. 2003; 278(14):12029–38. [PubMed: 12556532]

Letarte PB, Lieberman K, Nagatani K, Haworth RA, Odell GB, Duff TA. Hemin: levels in experimental subarachnoid hematoma and effects on dissociated vascular smooth-muscle cells. J Neurosurg. 1993; 79(2):252–5. [PubMed: 8331409]

Lu A, Tang Y, Ran R, Ardizzone TL, Wagner KR, Sharp FR. Brain genomics of intracerebral hemorrhage. J Cereb Blood Flow Metab. 2006; 26(2):230–52. [PubMed: 16034371]

Matsushita K, Meng W, Wang X, Asahi M, Asahi K, Moskowitz MA, Lo EH. Evidence for apoptosis after intercerebral hemorrhage in rat striatum. J Cereb Blood Flow Metab. 2000; 20(2):396–404. [PubMed: 10698078]

McGirt MJ, Parra A, Sheng H, Higuchi Y, Oury TD, Laskowitz DT, Pearlstein RD, Warner DS. Attenuation of cerebral vasospasm after subarachnoid hemorrhage in mice overexpressing extracellular superoxide dismutase. Stroke. 2002; 33(9):2317–23. [PubMed: 12215605]

Montesano R, Pepper MS, Mohle-Steinlein U, Risau W, Wagner EF, Orci L. Increased proteolytic activity is responsible for the aberrant morphogenetic behavior of endothelial cells expressing the middle T oncogene. Cell. 1990; 62(3):435–45. [PubMed: 2379237]

Nakamura M, Thourani VH, Ronson RS, Velez DA, Ma XL, Katzmark S, Robinson J, Schmarkey LS, Zhao ZQ, Wang NP, et al. Glutathione reverses endothelial damage from peroxynitrite, the byproduct of nitric oxide degradation, in crystalloid cardioplegia. Circulation. 2000; 102(19 Suppl 3):III332–8. [PubMed: 11082410]

Neekhra A, Luthra S, Chwa M, Seigel G, Gramajo AL, Kuppermann BD, Kenney MC. Caspase-8, -12, and -3 activation by 7-ketocholesterol in retinal neurosensory cells. Invest Ophthalmol Vis Sci. 2007; 48(3):1362–7. [PubMed: 17325185]

Oury TD, Piantadosi CA, Crapo JD. Cold-induced brain edema in mice. Involvement of extracellular superoxide dismutase and nitric oxide. J Biol Chem. 1993; 268(21):15394–8. [PubMed: 7687996]

Park S, Yamaguchi M, Zhou C, Calvert JW, Tang J, Zhang JH. Neurovascular protection reduces early brain injury after subarachnoid hemorrhage. Stroke. 2004; 35(10):2412–7. [PubMed: 15322302]

Phares TW, Fabis MJ, Brimer CM, Kean RB, Hooper DC. A peroxynitrite-dependent pathway is responsible for blood-brain barrier permeability changes during a central nervous system inflammatory response: TNF-alpha is neither necessary nor sufficient. J Immunol. 2007; 178(11): 7334–43. [PubMed: 17513784]

Qureshi AI, Tuhrim S, Broderick JP, Batjer HH, Hondo H, Hanley DF. Spontaneous intracerebral hemorrhage. N Engl J Med. 2001; 344(19):1450–60. [PubMed: 11346811]

Rincon F, Mayer SA. Novel therapies for intracerebral hemorrhage. Curr Opin Crit Care. 2004; 10(2): 94–100. [PubMed: 15075717]

Sagara J, Makino N, Bannai S. Glutathione efflux from cultured astrocytes. J Neurochem. 1996; 66(5): 1876–81. [PubMed: 8780013]

Saito A, Kamii H, Kato I, Takasawa S, Kondo T, Chan PH, Okamoto H, Yoshimoto T. Transgenic CuZn-superoxide dismutase inhibits NO synthase induction in experimental subarachnoid hemorrhage. Stroke. 2001; 32(7):1652–7. [PubMed: 11441215]

Sehba FA, Ding WH, Chereshnev I, Bederson JB. Effects of S-nitrosoglutathione on acute vasoconstriction and glutamate release after subarachnoid hemorrhage. Stroke. 1999; 30(9):1955–61. [PubMed: 10471450]

Sehba FA, Friedrich V Jr, Makonnen G, Bederson JB. Acute cerebral vascular injury after subarachnoid hemorrhage and its prevention by administration of a nitric oxide donor. J Neurosurg. 2007; 106(2):321–9. [PubMed: 17410718]

Shih AY, Johnson DA, Wong G, Kraft AD, Jiang L, Erb H, Johnson JA, Murphy TH. Coordinate regulation of glutathione biosynthesis and release by Nrf2-expressing glia potently protects neurons from oxidative stress. J Neurosci. 2003; 23(8):3394–406. [PubMed: 12716947]

Silva Y, Leira R, Tejada J, Lainez JM, Castillo J, Davalos A. Molecular signatures of vascular injury are associated with early growth of intracerebral hemorrhage. Stroke. 2005; 36(1):86–91. [PubMed: 15550687]

Szabo C, Mabley JG, Moeller SM, Shimanovich R, Pacher P, Virag L, Soriano FG, Van Duzer JH, Williams W, Salzman AL, et al. Part I: pathogenetic role of peroxynitrite in the development of diabetes and diabetic vascular complications: studies with FP15, a novel potent peroxynitrite decomposition catalyst. Mol Med. 2002; 8(10):571–80. [PubMed: 12477967]

Takano T, Tian GF, Peng W, Lou N, Libionka W, Han X, Nedergaard M. Astrocyte-mediated control of cerebral blood flow. Nat Neurosci. 2006; 9(2):260–7. [PubMed: 16388306]

Wang J, Dore S. Inflammation after intracerebral hemorrhage. J Cereb Blood Flow Metab. 2007; 27(5):894–908. [PubMed: 17033693]

Wasserman JK, Zhu X, Schlichter LC. Evolution of the inflammatory response in the brain following intracerebral hemorrhage and effects of delayed minocycline treatment. Brain Res. 2007

Willis CL, Nolan CC, Reith SN, Lister T, Prior MJ, Guerin CJ, Mavroudis G, Ray DE. Focal astrocyte loss is followed by microvascular damage, with subsequent repair of the blood-brain barrier in the apparent absence of direct astrocytic contact. Glia. 2004; 45(4):325–37. [PubMed: 14966864]

Wilson JX. Antioxidant defense of the brain: a role for astrocytes. Can J Physiol Pharmacol. 1997; 75(10–11):1149–63. [PubMed: 9431439]

Wu G, Fang YZ, Yang S, Lupton JR, Turner ND. Glutathione metabolism and its implications for health. J Nutr. 2004; 134(3):489–92. [PubMed: 14988435]

Zou CG, Agar NS, Jones GL. Enhancement of glutathione-dependent haemin degradation by ascorbic acid. Biochem Pharmacol. 2002; 64(4):565–72. [PubMed: 12167475]

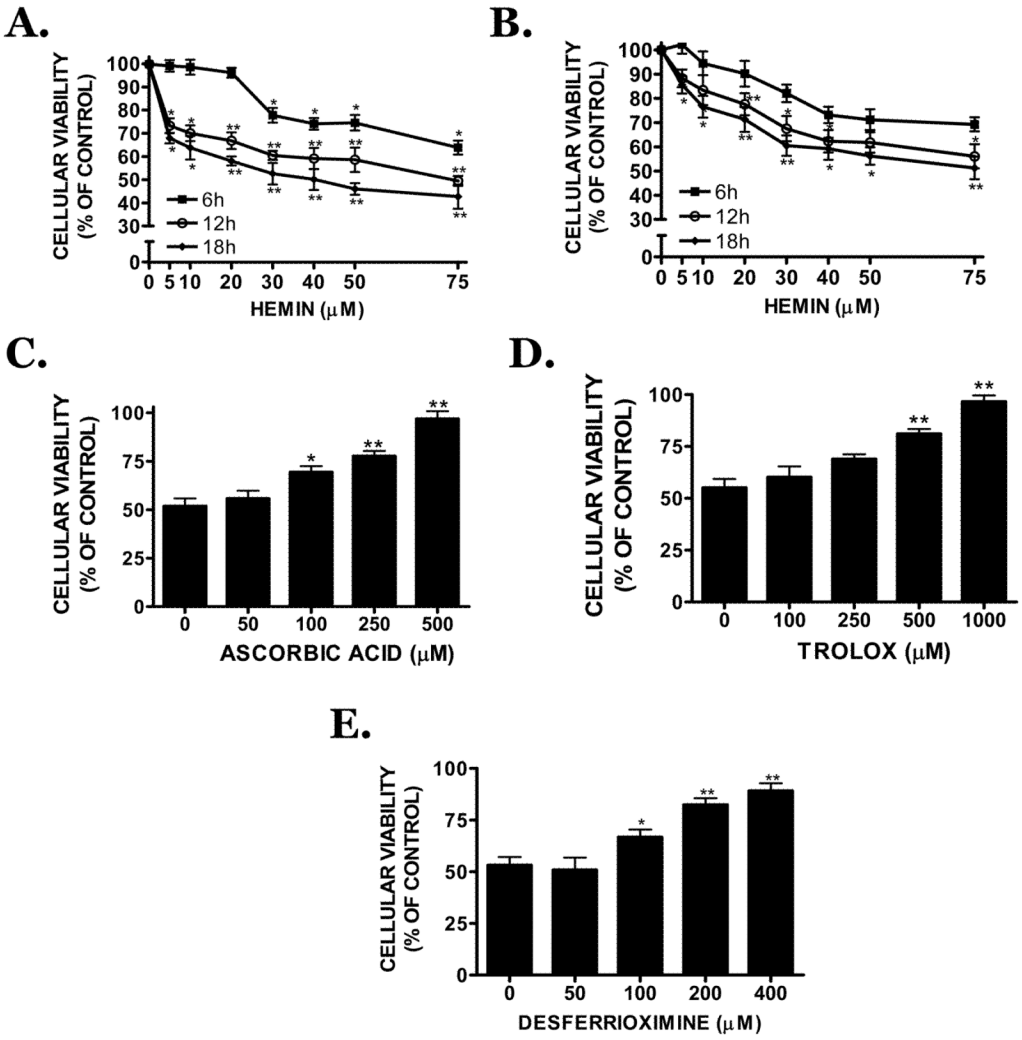

FIGURE 1.

Cellular viability was assessed using the MTT reduction assay in **(A)** mouse bEnd.3 or **(B)** human brain microvascular cells after a 6h, 12h, or 18h treatment with hemin (5–75 μM). Effect of the (**C)** antioxidant compounds, ascorbic acid, **(D)** trolox or (**E)** the iron chelating agent, desferrioxamine (DFO) on hemin (30 μM)-induced bEnd.3 cell death after an 18h treatment. Data are representative of three independent experiments (n=8/experiment). Data were analyzed using a One-Way ANOVA followed by Student-Newman-Keul's post-hoc test; * $p<0.05$, ** $p<0.01$ vs. vehicle-treated cultures.

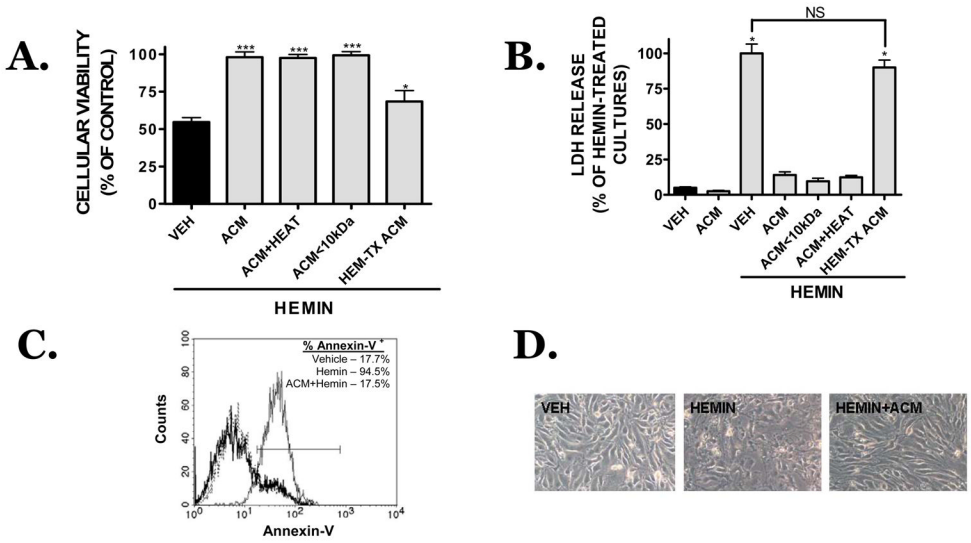

FIGURE 2.

Effect of ACM on hemin (30 μM, 18h)-induced cell death (VEH, black bar). Neither protein denaturation (ACM+HEAT) nor size exclusion ultrafiltration of proteins larger than 10 kDa (ACM<10 kDa) reduced the protective capacity of ACM, as assessed by **(A)** MTT assay or **(B)** LDH assay. In contrast, treatment of astrocytes with 30 μM hemin prior to the collection of ACM (HEM-TX ACM), reduced the observed vasculoprotection. Data are representative of three independent experiments (n=8/experiment). Data were analyzed using a One-Way ANOVA followed by Student-Newman-Keul's post-hoc test; * $p<0.05$ vs. vehicle-treated cultures, NS = not significantly different. **(C)** Quantification of apoptotic cell death, as assessed by Annexin V-PE staining, following an 18h treatment with vehicle (thick black line), hemin (30 μM; thin black line) or hemin+ACM treatment (dotted line). (**D)** Morphology of bEnd.3 cells after vehicle (VEH), hemin (HEMIN) or hemin+ACM (HEMN +ACM) treatment.

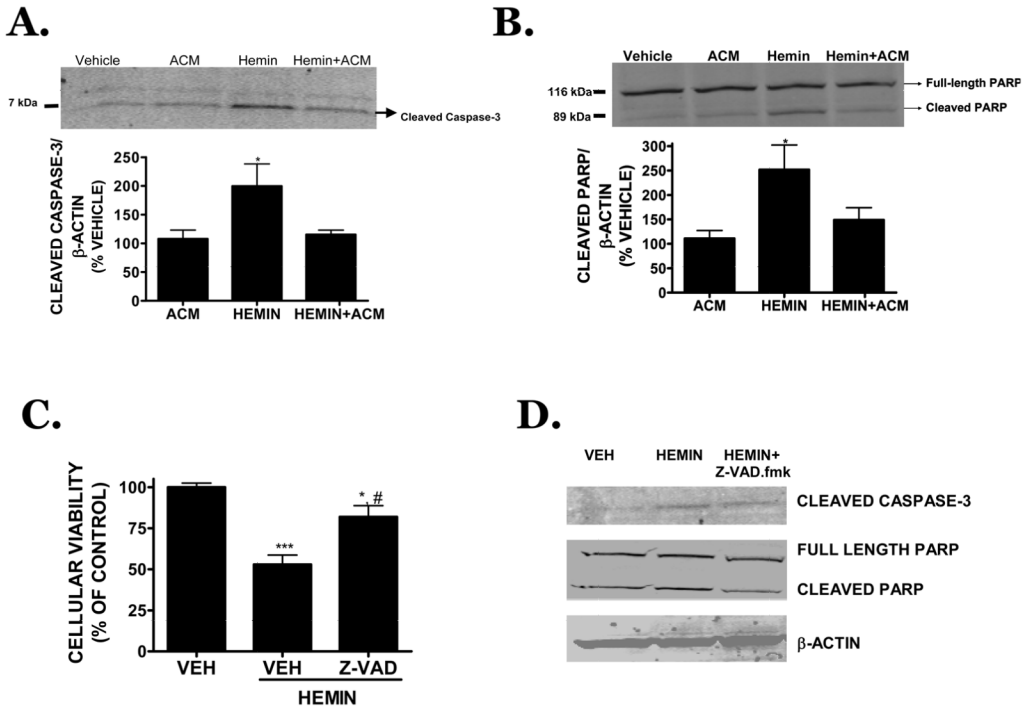

FIGURE 3.

(A) Representative Western blot of cleaved caspase-3 after an 18h treatment with 30 μM hemin in the presence or absence of ACM. Densitometry from independent experiments is provided below the blot. **(B)** Representative Western blot of cleaved PARP, a downstream substrate of activated caspase-3 and hallmark of apoptotic cell death, following an 18h treatment with 30 μM hemin in the presence or absence of ACM. Densitometry from independent experiments is provided below the blot. **(C)** Effect of the irreversible, pan-caspase inhibitor, Z-VAD.fmk (100 μM) on 30 μM hemin-induced cell death following an 18h treatment in bEnd.3 cells. **(D)** Effect of Z-VAD.fmk (100 μM) on 30 μM hemin-induced caspase-3 activation and PARP cleavage following an 18h treatment in bEnd.3 cells. For all studies, data are representative of three independent experiments (n=6/experiment). Data were analyzed using a One-Way ANOVA followed by Dunnett's post-hoc test; * $p<0.05$, *** $p<0.001$ vs. vehicle-treated cultures.

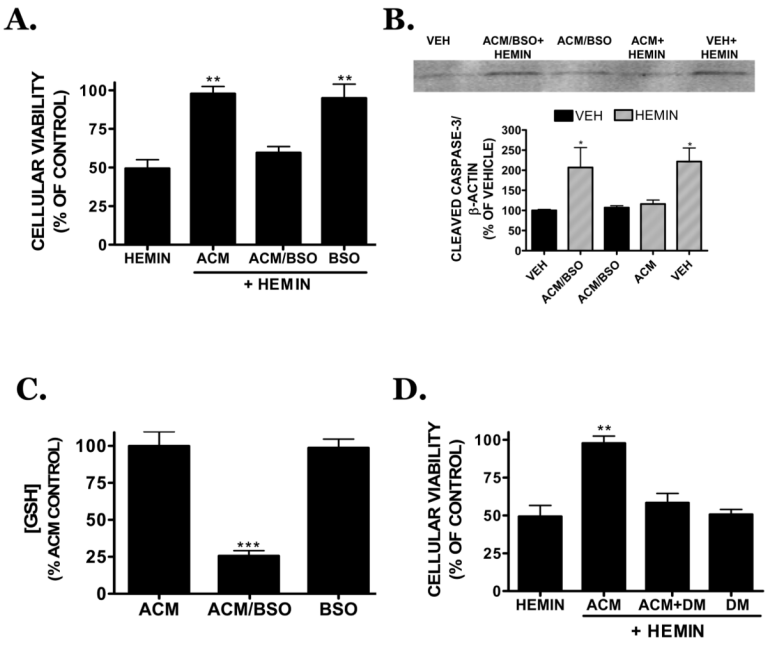

FIGURE 4.

(A) Effect of ACM on hemin (30 μM)-induced cell death following an 18h exposure in bEnd.3 cells. The GSH depleting agent, DL-buthionine (S,R)-sulfoximine (BSO; 1 mM, 8h treatment), eliminated the protective capacity of ACM when added to astrocytes prior to ACM collection (ACM/BSO), but not when directly added to previously collected ACM (BSO). **(B)** Hemin-induced caspase-3 activation was reversed by co-treatment with ACM in bEnd.3 cells whereas treatment of astrocyte cultures with BSO prior to ACM collection (ACM/BSO) eliminated the reduction in caspase-3 activation. ACM/BSO alone had no effect on caspase-3 activation (black bar) or cellular viability (data not shown). Hemin-treated groups are depicted by hatched bars. Representative Western blot is shown with densitometry from three independent experiments. **(C)** Effect of BSO (1 mM) on GSH content within ACM. Direct addition of 1 mM BSO to previously collected ACM (BSO; grey bar) did not affect GSH levels. **(D)** Effect of diethyl maleate (ACM+DM; 300 μM), a thiol-depleting agent, on ACM-mediated protection after an 18h treatment with hemin (30 μM). Data are representative of three independent experiments (n=6/experiment). Data were analyzed using a One-Way ANOVA followed by Dunnett's post-hoc test; ** $p<0.01$ vs. vehicle-treated cultures.

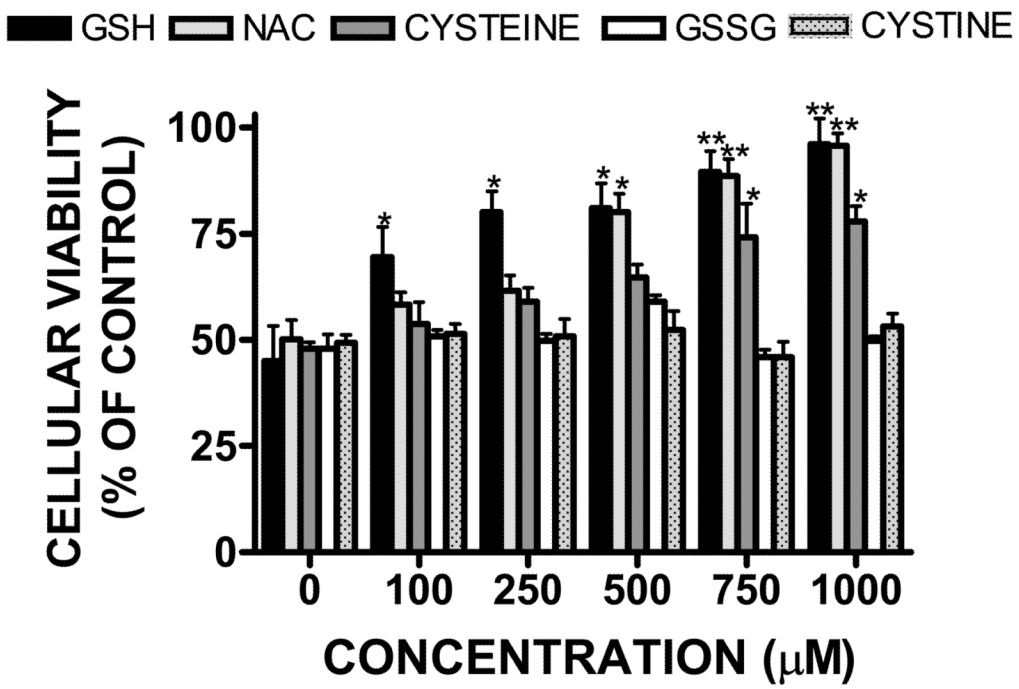

FIGURE 5.

Concentration-dependent reduction in hemin (30 μM)-induced microvessel cell death following an 18h co-treatment with GSH (0–1000 μM), the GSH precursor drug, N-acetyl-L-cysteine (NAC), the GSH precursor, cysteine, oxidized glutathione (GSSG), or with cystine. Data are representative of three independent experiments (n=6/experiment). Data were analyzed using a One-Way ANOVA followed by Dunnett's post-hoc test; * $p < 0.05$, ** $p < 0.01$ vs. hemin treated cultures (0 μM).

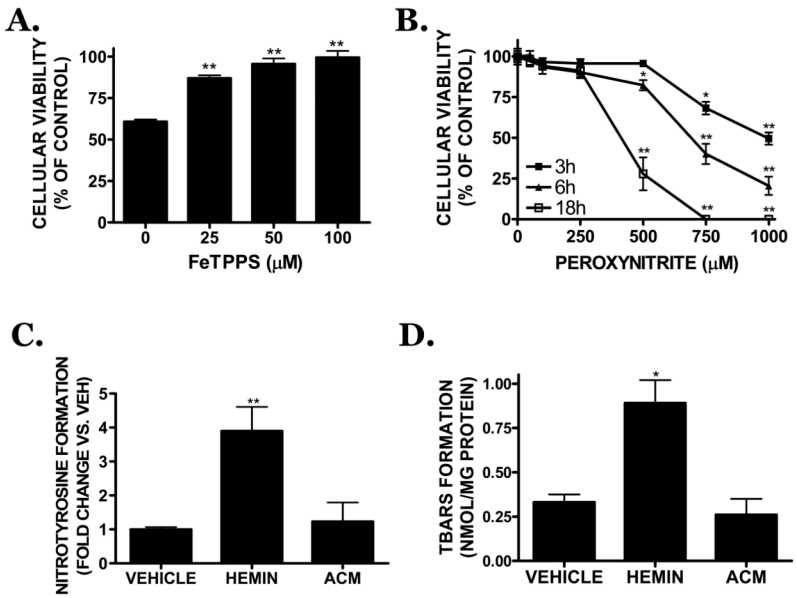

FIGURE 6.

(A) The peroxynitrite decomposition catalyst, FeTPPS (25–100 μM) reduced 30 μM hemin-induced cell death after an 18h treatment in bEnd.3 cells. **(B)** Exogenous peroxynitrite (250–1000 μM) increased cell death in a time- and concentration-dependent manner. Hemin (30 μM; HEMIN)-induced **(C)** nitrotyrosine formation, a marker of peroxidative injury, or **(D)** TBARS formation, a measure of lipid peroxidation, were attenuated by co-treatment with ACM. Data are representative of at least three independent experiments (n=6/experiment). Data were analyzed by One-Way ANOVA followed by Dunnett's post-hoc test; * $p< 0.05$, ** $p<0.01$ vs. hemin treated cultures (0 μM).

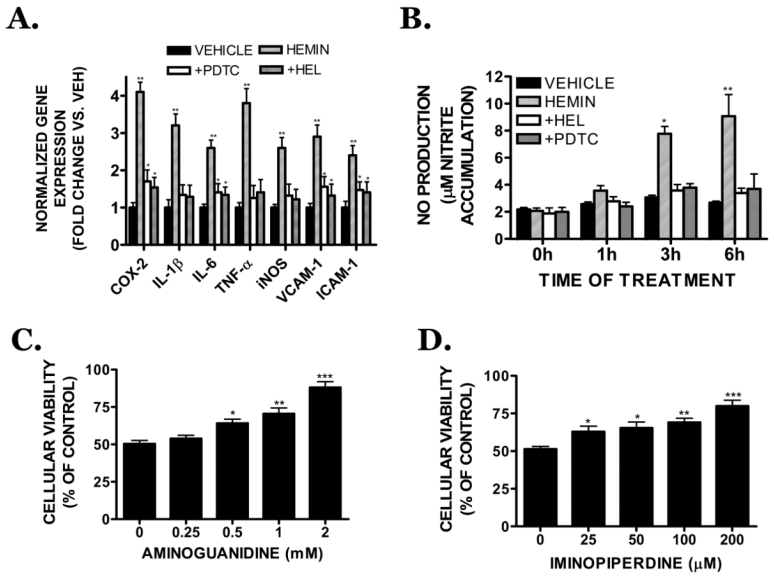

FIGURE 7.

(A) Effect of the NFκB inhibitor, PDTC (100 μM) or the p65 translocation inhibitor, helanalin (10 μM) on 30 μM hemin-induced inflammatory gene expression (cyclooxygenase-2 (COX-2), interleukin-1β (IL-1β), interleukin-6 (IL-6), tumor necrosis factor-α (TNF-α), inducible nitric oxide synthase (iNOS), vascular cell adhesion molecule-1 (VCAM-1) or intercellular cell adhesion molecule-1 (ICAM-1)) following an 18h treatment in bEnd.3 cells. Data were normalized to the housekeeping gene, RPS3, and are expressed as fold change vs. vehicle-treated cultures. Data are the mean ± SEM of three independent trials (n=3/trial). **(B)** Effect of PDTC and helenalin on nitrite formation after a 1–6h treatment with 30 μM hemin. Effect of the selective iNOS inhibitors **(C)** aminoguanidine (0.25–5 mM) or **(D)** 2-iminopiperdine (25–200 μM) on hemin-induced cell death after an 18h treatment. Data are representative of three independent experiments (n=6/experiment) and were analyzed by One-Way ANOVA followed by Dunnett's post-hoc test; * $p < 0.05$, ** $p<0.01$, *** $p<0.001$ vs. hemin treated cultures (0 μM).

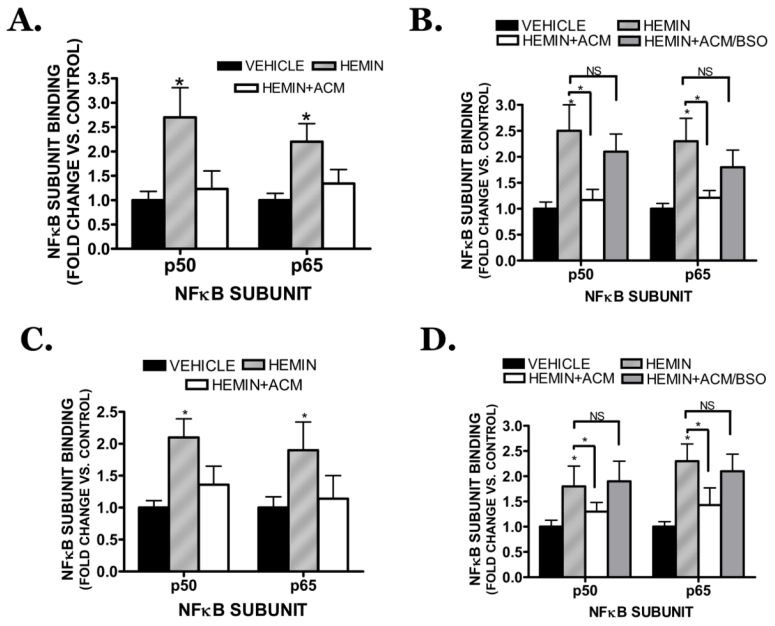

FIGURE 8.

(A) Effect of ACM on hemin (30 μM)-induced NFκB (p50 or p65 subunit) activation in bEnd.3 cells following a 2h treatment. **(B)** Hemin-induced NFκB activation is attenuated by ACM whereas ACM collected from astrocytes previously incubated with BSO (ACM/BSO) did not significantly reduce either p50 or p65 activation. **(C)** ACM collected from human astrocytes significantly attenuated hemin-induced NFκB activation in human brain microvascular cells after a 2h treatment. **(D)** Hemin-induced NFκB activation in human brain microvascular cells is attenuated by ACM from human astrocytes whereas ACM collected from astrocytes previously incubated with BSO (ACM/BSO) did not significantly reduce either p50 or p65 activation. Data are representative of at least three independent trials and were analyzed using a One-Way ANOVA followed by Dunnett's post-hoc test; * $p < 0.05$ vs. hemin treated cultures, NS=not significantly different.

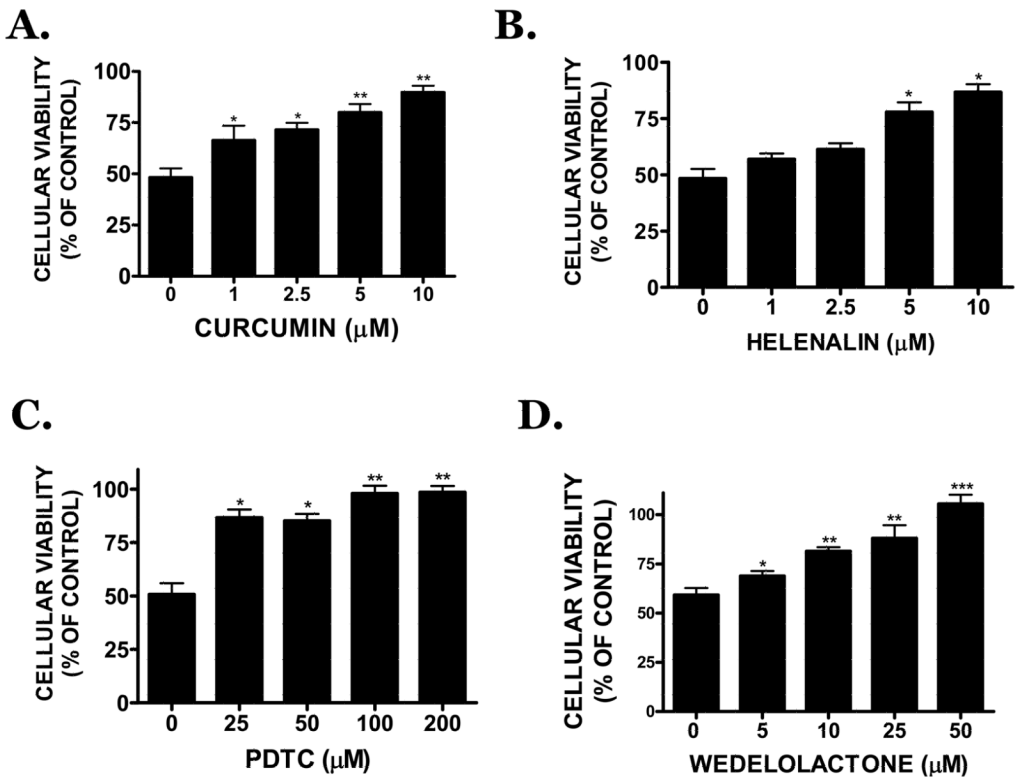

FIGURE 9.

B) Effect of the NFκB pathway inhibitors, **(A)** curcumin (1–10 μM), **(B)** PDTC (25–200 μM), **(C)** helenalin (1–10 μM) or **(D)** wedelolactone (5–50 μM) on 30 μM hemin-induced cell death following an 18h treatment. Data are representative of three independent experiments (n=6/experiment) and were analyzed using a One-Way ANOVA followed by Dunnett's post-hoc test; * $p<0.05$, ** $p<0.01$, ***$p<0.001$ vs. hemin treated cultures.